Available online at www.sciencedirect.com

ScienceDirect

Procedia CIRP 108 (2022) 845–850

www.elsevier.com/locate/procedia

6th CIRP Conference on Surface Integrity (CSI 2022)

# Characterization of friction for the simulation of multi-pass orthogonal micro-cutting of 316L stainless steel

N. Fezai, L. Chaabani*, N.F. Niang, M.H. Bin Haamsir, M. Fontaine, A. Gilbin, P. Picart

*FEMTO-ST Institute, UMR CNRS 6174, Univ. Bourgogne Franche Comté – UBFC (ENSMM/UFC), F-25000 Besançon, France*

* Corresponding author. Tel.: +33 381 666 000 ; fax: +33-381 666 700. *E-mail address:* lobna.chaabani@femto-st.fr

**Abstract**

Contact behavior at the tool-workpiece and the tool-chip interface affects the machined surface integrity, and it is especially significant in micromachining. In order to predict surface integrity in multi-pass orthogonal micro-cutting from numerical simulation, it is important to define the contact between these different surfaces. In this article, contact in micro-cutting of the 316L stainless steel with a tungsten carbide tool is investigated within tribology tests at different sliding velocities combined with numerical simulation in order to study the evolution of the friction coefficient. Finally, a friction coefficient function of sliding velocity is integrated in orthogonal micro-cutting finite element model and its relevance in the context of multi-pass micro-cutting is discussed.



*Keywords:* Friction, Sliding velocity, Micro-cutting.

## 1. Introduction

Mechanical micro-fabrication is a field that has developed widely in recent decades. It includes now numerous processes such as additive manufacturing (metal, ceramic or polymer), micro-injection (polymers, charged or not with particles), plastic deformation processes (stamping, cutting, etc.), micro-machining (milling, turning, EDM, etc.). The latter has varied applications: optics, electronics, luxury products, medical device, or even as a finishing step for all the other processes.

Among the micro-machining processes, micro-cutting is a real issue. It has many advantages: high chip flow, complexity of the surfaces that can be machined and a wide range of adapted materials. Steel, copper alloys and aluminum alloys represent three quarter of material used in micro-milling (mainly steels: 40%) [1]. They are used for electrodes and micro-imprints for plastic injection. Stainless steel and titanium alloys are most of the time used for biomedical field. It offers complex geometry components with low tolerances, but it is difficult to master because of size effects. To investigate these effects due to under-scaling, researchers use both experimental and numerical methods.

The experimental way is expensive, so the numerical simulation can represent a solution to understand the different size effects, to predict them, and to limit experimental tests to be done. However, to obtain a reliable numerical model of micro-cutting process, a better understanding of friction behavior is necessary. So far, the Coulomb model with a constant coefficient, irrespective of temperature and pressure, is usually used to simulate the friction phenomena at the tool-chip-workpiece contact interface. In fact, the contact at these different interfaces is a function of multiple parameters such as temperature, sliding velocity and contact pressure [2, 3], so the assumption of a constant coefficient along the interface is not consistent.

The purpose of this paper is to identify a new friction model to better describe the contact behaviour between the tool-chip interface and the tool-workpiece interface during the cutting of AISI 316L work-piece with WC-Co tool.

## 2. Friction experiments

### 2.1. Experimental set-up

A conventional pin-on-surface testing tribometer system is used in order to estimate apparent friction coefficient along the tool-chip-work-piece contact interface. The system is mounted on a 4-axes DOOSAN© lathe in ENSMM workshop. The experimental set-up is illustrated in Fig. 1. A cylindrical bar made of the same grade of machined material AISI 316L is fixed onto the lathe's chuck. A 5 mm diameter ball made of WC-Co (cutting tool material) is pressed onto the cylindrical surface by the means of a jack forming a sphere-cylinder contact.

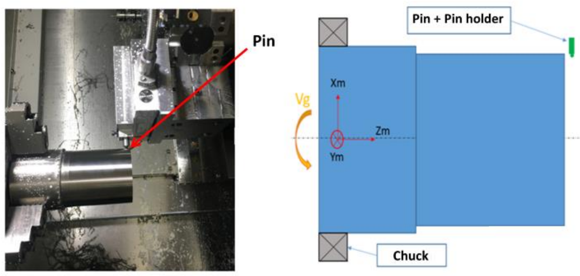


Fig. 1. Pin-on-cylinder tribometer in a lathe.

2212-8271 © 2022 The Authors. Published by Elsevier B.V.

10.1016/j.procir.2022.03.130

The friction test is divided into two steps. At first, the pin penetrates onto the cylindrical surface incrementally as the normal force can be fixed to a static reference value by controlling the penetration depth. Secondly, the bar starts a rotational movement and the pin an axial feed in Z+ direction along the cylinder. The use of the lathe provides a wide range of sliding velocities. After each friction test, the same cutting tool refreshes the surface ploughed by the pin with the same feed in all cases. So we have the same surface roughness in all tests. The pin-holder is fixed onto a dynamometer in order to measure the normal ($F_n$) and tangential ($F_t$) forces (macroscopic forces). The used dynamometer is a 3–components Kistler© 9129AA.

### *2.2. Testing parameters*

The sliding velocity is variable along the tool-chip-workpiece contact [2]. The range of sliding velocity chosen during this study varies between 10 and 160 m/min in order to understand the tribological behavior at the different tool-workpiece-chip interfaces (secondary shear zone, tertiary shear zone and flank zone). Thanks to the configuration of the tribometer we can perform friction tests at wide range of velocities.

FE model of orthogonal micro-cuting shows that, During micro-cutting contact pressure varies between 2000 MPa and 3000 MPa. A normal force equal to 450 N leading to an average pressure 2500 MPa, has been applied onto pins in order to be consistent with preliminary turning tests into the same material.

### *2.3. Experimental results*

Tangential and normal forces are the online outputs provided by this experimental set-up (Fig. 2). To insure results accuracy each friction test is repeated twice. The average of normal and tangential forces over two consectutive tests presents a deviation less than 5%. The ratio between tangential and normal force can be defined as the apparent friction coefficient.

$$\mu_{app} = \frac{Ft}{Fn} \qquad (1)$$

The evolution of $\mu_{app}$ for different sliding velocities is plotted in Fig.3.

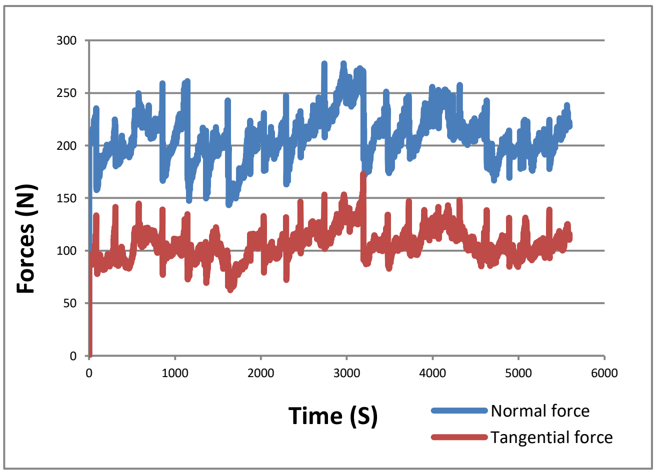


Fig. 2. Evolution of normal and tangential forces during friction test.

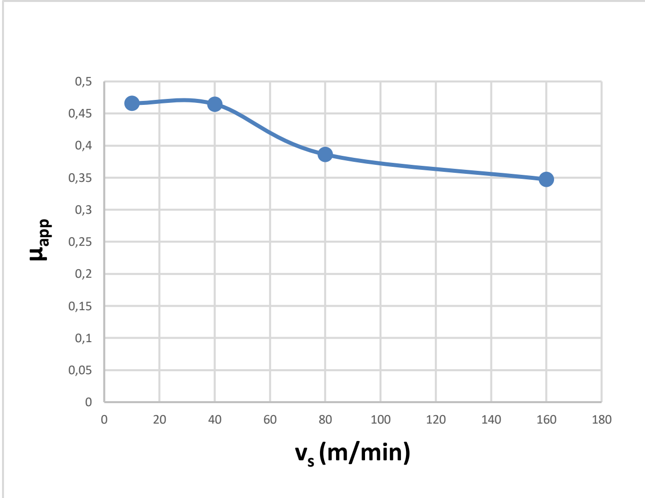


Fig. 3. Apparent friction coefficient depending on the sliding velocity.

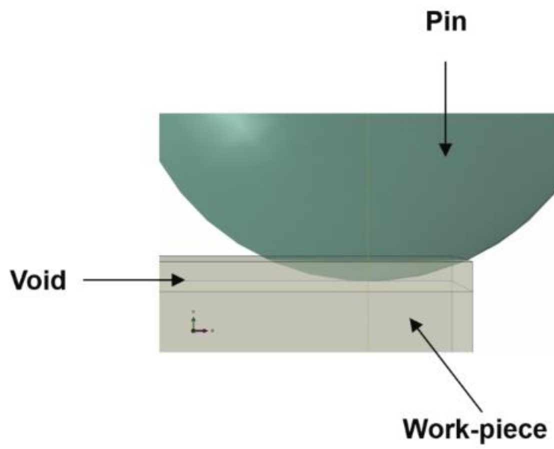


Fig. 4. Configuration of the CEL numerical model.

We can notice from the Fig. 3, that friction is influenced by sliding velocity so we can no longer consider that the friction is independent from sliding velocity.

We suppose that apparent friction coefficient decreases due to the increase in temperature generated by the increase in the velocity. Wording, the increase of temperature leads to a thermal softening hence fluid-type friction.

## 3. Friction model identification

### *3.1. Introduction*

The apparent friction coefficient results from an adhesive phenomena and the plastic deformation of the workpiece material induced by the pin under high pressure.

The adhesive part can be only investigated using numerical modeling of friction test. Hence, a numerical model of friction allows us to identify the adhesive friction behavior in the range of (10 - 160 m/min) and to estimate the indentation depth and then check contact area and average contact pressure. For this purpose, a finite element model simulating the friction test has been developed using CEL (Coupled Eulerian Lagrangian) method. From a general point of view, this type of model is composed of an Eulerian mesh representing the volume in which the Eulerian material (the workpiece) "flows" and interacts with Lagrangian part (the pin) as shown in Fig. 4.

### 3.2. Model description

A 3D-model of friction test has been developed with ABAQUS© explicit. There was no thermo-mechanical coupling for simplification reasons. The thermal aspect will be taken into account in further work.

#### 3.2.1. The Pin

The pin is presented by a half-sphere with a diameter of 5 mm and its material is WC-Co. It uses Tetrahedral C3D4T elements and is considered as a rigid body where a reference point is defined in order to manage its displacement. The mechanical properties of WC-Co are provided in Table 1.

Table 1. Mechanical properties of WC-Co [3]

| Young's modulus (MPa) | Poisson's ratio | Temperature (K) |
|---|---|---|
| 368000 | 0.25 | 293.15 |
| 387000 | 0.25 | 373.15 |
| 364000 | 0.25 | 573.15 |
| 298000 | 0.25 | 773.15 |
| 192000 | 0.25 | 973.15 |
| 110000 | 0.25 | 1173.15 |

#### 3.2.2. The workpiece

The workpiece made of AISI 316L is presented by an eulerian part which flows in the eulerian domain. Element type used is 3D, rectangular, Eulerian with linear displacement.
The mechanical properties of the AISI 316L are reported in Table 2 [4].

Table 2. Mechanical properties of AISI 316L [4]

| Young's modulus (MPa) | Poisson's ratio | Temperature (K) |
|---|---|---|
| 210290 | 0.3 | 293.15 |
| 191670 | 0.3 | 423.15 |
| 179950 | 0.3 | 533.15 |
| 190980 | 0.3 | 623.15 |
| 188220 | 0.3 | 698.15 |
| 186150 | 0.3 | 753.15 |
| 156510 | 0.3 | 813.15 |
| 113760 | 0.3 | 923.15 |
| 68000 | 0.3 | 1473.15 |

In order to describe the material flow, a Johnson-Cook flow law has been used, eq (2). This model is dependent on strain, strain rate and temperature. In our study, the temperature is neglected due to simplification reasons.

$$\sigma = [A + B\varepsilon^n] \times \left[1 + C\, ln\frac{\dot{\varepsilon}}{\dot{\varepsilon}_0}\right] \times \left[1 - \left(\frac{\theta-\theta_t}{\theta_{fusion}-\theta_t}\right)^m\right] \quad (2)$$

Where $A$ is yield strength (MPa) ; $B$ is hardening modulus (MPa) ; $C$ is strain rate sensitivity coefficient ; $n$ is hardening coefficient ; $m$ is thermal softening coefficient ; $\dot{\varepsilon}$ is plastic strain rate ( $s^{-1}$ ) ; $\dot{\varepsilon}_0$ is reference plastic strain rate ( $s^{-1}$ ) ; $\theta_{fusion}$ is melting temperature of the workmaterial (K) ; $\theta$ is temperature of the work-material (K) and $\theta_0$ is room temperature (K). The values of these parameters are given in Table 3 [3].

Table 3. Johnson-Cook law's parameters [4]

| A (MPa) | B (MPa) | n | m | c | Melting T (K) | Transition T (K) |
|---|---|---|---|---|---|---|
| 453 | 402 | 0.47 | 0.77 | 0.36 | 1793.15 | 293.15 |

#### 3.2.3. Contact modeling

The contact behavior between the pin and the workpiece has been modeled by a Coulomb friction model. In fact, the adhesive friction coefficient $\mu_{adh}$ can be introduced. For constant pressure and sliding velocity, $\mu_{adh}$ is constant which describes the contact between the pin and the workpiece.
The relation between the friction stress $\tau_f$ and the normal stress $\sigma_n$ is described by eq. (3)

$$\tau_f = \mu_{adh}.\sigma_n \quad (3)$$

Basing on Bowden & Tabor [4], we assume that:

$$\mu_{app} = \mu_{adh} + \mu_{plast} \quad (4)$$

Where $\mu_{plast}$ describes the plastic deformation during cutting and $\mu_{adh}$ corresponds to the adhesive behavior of the contact.

#### 3.2.4. Boundary conditions

Different surfaces of the domain are blocked as shown in Fig. 5 along calculation.

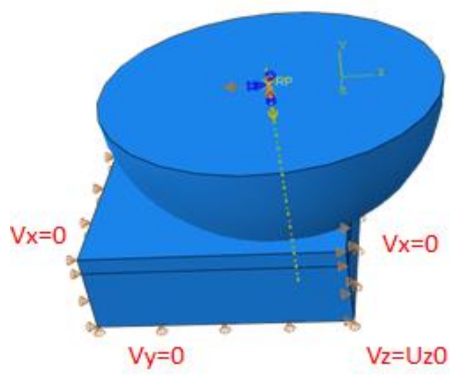


Fig. 5. Boundary conditions of the CEL model.

As in experiments, the model is divided into two motion steps:

- Indentation: The pin moves in –Y direction in order to indent the work-piece.
- Sliding: The pin moves in –X direction with the sliding velocity Vs.

## 4. Model readjustment

All parameters used in the numerical model are found in bibliography except the indentation depth and the adhesive friction coefficient. The aim of this work is to look for the depth of indentation and the adhesive coefficient of friction $\mu_{adh}$ values by combining numerical and experimental friction tests where tangential force, normal force and apparent friction coefficient values are provided by the experimental set-up. For every condition simulated by the developed model, an iterative method was developed in order to be in the same configuration than in experiments. This method is based on two independent steps that consists of identifying:

-The indentation depth in order to obtain $F_{n\ exp}$.

$$F_{n\ exp}=F_{n\ num} \tag{5}$$

-The adhesive friction coefficient in order to obtain numerical apparent friction coefficient equal to experimental apparent friction coefficient.

$$\mu_{app\ exp}=\mu_{app\ num} \tag{6}$$

## 5. Numerical results

### *5.1. Friction coefficients*

Comparisons between experimental and numerical values of normal force and apparent friction coefficient for different sliding velocity (10, 40, 80 and 160 m/min) are plotted respectively in Fig.6 and Fig.7. the figures show that deviation between experimental and numerical values is less than 3%. As consequence, we can admit that the numerical model can be employed to obtain quantitative results.

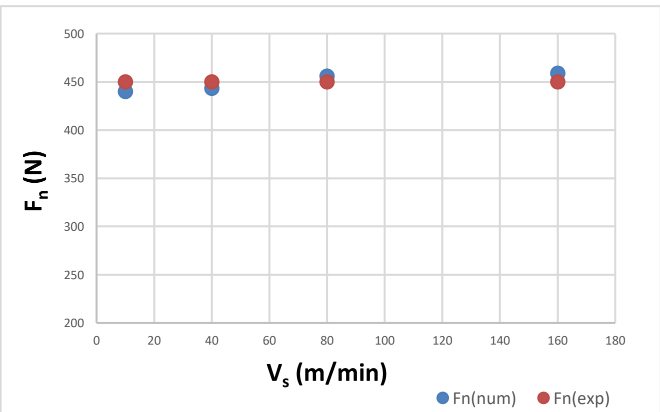


Fig. 6. Comparison between experimental and numerical results of normal force.

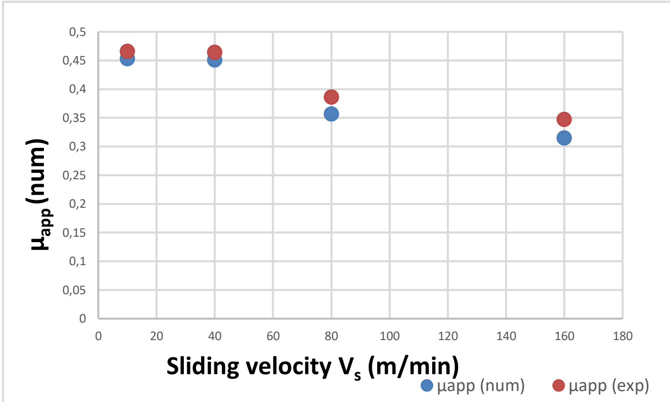


Fig. 7. Evolution of numerical and experimental coefficient of friction with the sliding velocity.

Bowden & Tabor [5] estimate that the major part of friction is adhesive. From Fig.8, it can be noticed that the adhesive part of apparent friction occupies 80 to 90% of apparent friction coefficient. As result, the presented friction test allows for the investigation of adhesion.

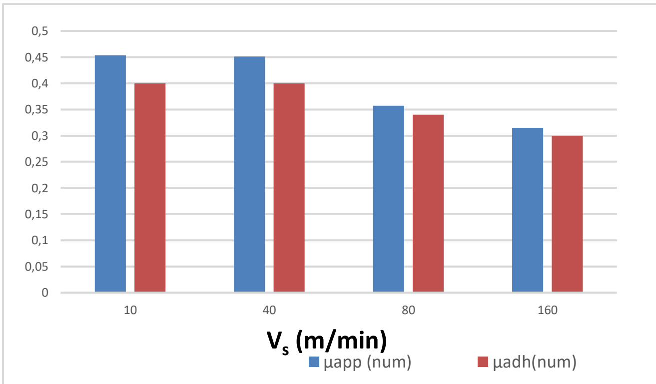


Fig. 8. Proportion of plastic deformation and adhesion during friction tests for each sliding velocity.

### *5.2. Local sliding velocity*

The numerical model provides as output values of local sliding velocity at pin-workpiece interface. Fig.9 shows that local sliding velocity at pin-workpiece interface is reduced. This proves that adhesion limits the sliding velocity.

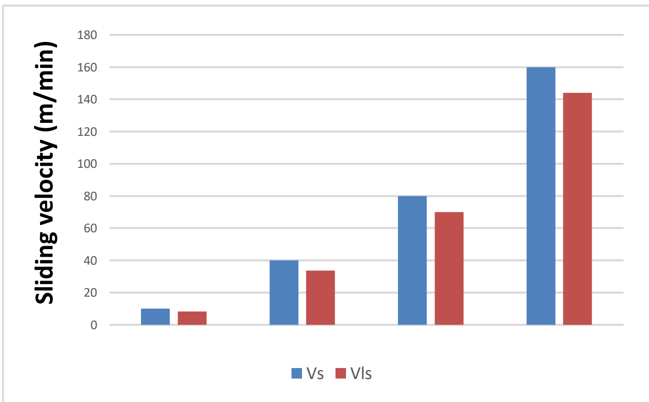


Fig. 9. Comparison between the average local sliding velocity $V_{ls}$ and the macroscopic sliding velocity $V_s$.

For sliding velocities (macroscopic) $V_s$= 10, 40, 80, 160 m/min, the correspondent local sliding velocities (material flow velocity) are $V_{ls}$=8, 33, 70, 140 m/min.

*5.3. Friction depending on local sliding velocity*

According to Bonnet et al. [6], the local sliding velocity along the tool-workpiece-chip interface is variable. Fig. 10 shows the evolution of local sliding velocity along the contact during metal cutting with cutting velocity $V_c$=120 m/min. The friction behavior can be divided in 3 zones:

- A-B: the friction behavior on clearance face of the tool is a sliding one, which explains the increase of local sliding velocity value until reaching the cutting velocity.
- B-B': the friction behavior on the tip of the tool is a sticking one, which explains low values of local sliding velocity.
- B'-C: the friction behavior on the rake face is a sliding one, which explains high values of local sliding velocity.

A friction model depending on local sliding velocity seems to be relevant to describe the frictional behavior on tool-chip-workpiece interfaces. According to this model, coefficient of friction is no longer constant but it varies along chip-tool-workpiece interfaces. It helps to describe the frictional behavior during micro-cutting which allows the development of reliable finite element model of micro-cutting. The aim is to study the different aspect of micro-cutting in general and multi-pass micro-cutting in particular. Fig.11 shows the evolution of adhesive friction coefficient for local sliding velocity between 8 and 140 m/min corresponding to macroscopic sliding velocity between 10 and 180 m/min. From the curve plotted on Fig.11, an equation linking adhesive friction coefficient and local sliding velocity in the range of 8-120 m/min is extracted:

$$\mu_{adh} = -0.023\, V_{ls} + 0.43 \quad (7)$$

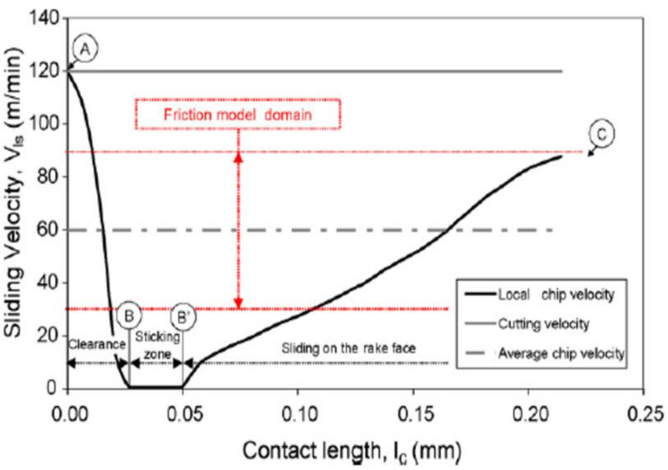


Fig. 10. Example of FE models using the new friction model [6].

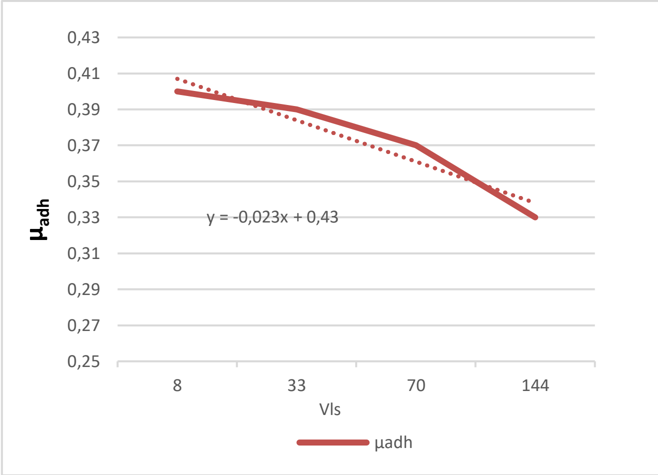


Fig. 11. Evolution of the adhesive friction coefficient depending on local sliding velocity $V_{ls}$.

## 6. Conclusions and prospects

This work presents a model linking adhesive friction coefficient and local sliding velocity. It is evident that this model provides a better description of friction behavior along the tool-chip-workpiece interface comparing to the Coulomb model. Nevertheless, it is still incomplete. It is a fact that pressure and temperature have a huge effect on the frictional behavior. From the other hand, experimental data used in this study are not sufficient to cover the majority of sliding velocity range.

This friction model can be integrated in orthogonal microcutting finite element model and would be relevant for multi-pass micro-cutting modeling after taking into account of temperature dependency.

A good description of friction behavior during the cut makes it possible to properly describe the flow of material around the tool, and then model the machined surface by presenting residual stresses. According to literature, residual stress affects the machined surface integrity, which can influence fatigue resistance of, machined components. In addition, it is known that multi-pass cutting increase compressive residual stress in the machined surface, which makes a finite element model of multi-pass micro-cutting process very important.

In further works:

- Friction tests, giving information about temperature and forces, will be carried out in a wider range of sliding velocities.
- Friction model correlation will be done also through cutting tests.
- The obtained friction law will be implemented in a multi-pass CEL FEM model of micro-cutting.

## References

[1] M.A. Camara, J.C. C.Rubio, A.M. Abrao, J.P. Davim « State of the Art on Micromilling of Materials » *Journal of Materials Science & Technology*, vol. 28, pp. 673–685, 2012.

[2] J. Rech, « A multiview approach to the tribological characterization of cutting tool coatings for steels in high-speed dry turning » *International Journal for Machining and Machinability of Materials*, vol. 1, pp. 27–44, 2006.

[3] P.K. Wright, E.M. Trent, Metal Cutting, London: Butterworth Heinemann, 2000.

[4] T. Mabrouki, J-F. Rigal, « A contribution to a qualitative understanding of thermo-mechanical effects during chip formation in hard turning » *Journal of Materials Processing Technology,* vol. 176, pp. 214-22, 2006.

[5] F. Bowen, D. Tabor, Friction and Lubrication of Solids, Oxford: Oxford University Press, 1951.

[6] C. Bonnet, F. Valiorgue, J. Rech, C. Claudin, H. Hamdi, J.M. Bergheau, P. Gilles, « Identification of a friction model—Application to the context of dry cutting of an AISI 316L austenitic stainless steel with a TiN coated carbide tool » *International Journal of Machine Tools & Manufacture,* vol. 48, pp. 1211-1223, 2008.